

Adversarially Robust Prototypical Few-shot Segmentation with Neural-ODEs

Prashant Pandey^{*1}[0000-0002-6594-9685], Aleti Vardhan^{*2}, Mustafa Chasmai¹,
Tanuj Sur³, and Brejesh Lall¹

¹ Indian Institute of Technology Delhi, India

² Manipal Institute of Technology, India

³ Chennai Mathematical Institute, India

getprashant57@gmail.com

Abstract. Few-shot Learning (FSL) methods are being adopted in settings where data is not abundantly available. This is especially seen in medical domains where the annotations are expensive to obtain. Deep Neural Networks have been shown to be vulnerable to adversarial attacks. This is even more severe in the case of FSL due to the lack of a large number of training examples. In this paper, we provide a framework to make few-shot segmentation models adversarially robust in the medical domain where such attacks can severely impact the decisions made by clinicians who use them. We propose a novel robust few-shot segmentation framework, Prototypical Neural Ordinary Differential Equation (PNODE), that provides defense against gradient-based adversarial attacks. We show that our framework is more robust compared to traditional adversarial defense mechanisms such as adversarial training. Adversarial training involves increased training time and shows robustness to limited types of attacks depending on the type of adversarial examples seen during training. Our proposed framework generalises well to common adversarial attacks like FGSM, PGD and SMIA while having the model parameters comparable to the existing few-shot segmentation models. We show the effectiveness of our proposed approach on three publicly available multi-organ segmentation datasets in both in-domain and cross-domain settings by attacking the support and query sets without the need for ad-hoc adversarial training.

Keywords: Few-shot Segmentation· Neural-ODE· Adversarial Robustness.

1 Introduction

Modern day safety-critical medical systems are vulnerable to different kinds of attacks that can cause danger to life. With the penetration of AI, Machine Learning and Deep Neural models to healthcare and medical systems, it is imperative

* equal contribution

to make such models robust against different kinds of attacks. By design, these models are data-hungry and need a significant amount of labelled data to improve their performance and generalizability. Past studies have shown that it is not always feasible to annotate medical data, especially for segmentation problems due to the huge time and specific skills it needs to do so. Lack of well-annotated data, make these models vulnerable to different kind of attacks like adversarial white and black box attacks [2,5,13] on Deep Neural models. ML practitioners employ FSL [7,1] to learn patterns using well-annotated base classes, finally to transfer the knowledge to scarcely annotated novel classes. This knowledge transfer is severely impacted in the presence of adversarial attacks when *support* and *query* samples from novel classes are injected with adversarial noise [29].

Commonly used Adversarial Training mechanisms [2,13,17] require adversarially perturbed examples shown to the model during training. [34] introduced standard adversarial training (SAT) procedure for semantic segmentation. These methods do not guarantee defense when the type of attack is different from the adversarially perturbed examples [18,30] and it is impractical to expose the model with different kind of adversarial examples during training itself. Also, a common method that handles attacks both on support and query examples of novel classes, is non-existent. To the best of our knowledge, the adversarial attacks on few-shot segmentation (FSS) with Deep Neural models and their defense mechanisms have not yet been explored and the need for such robust models is inevitable. To this end, we propose **Prototypical Neural Ordinary Differential Equation (PNODE)**, a novel prototypical few-shot segmentation framework based on Neural-ODEs [14] that provides defense against different kinds of adversarial attacks in different settings. Owing to the fact that the integral curves of Neural-ODEs are non-intersecting, adversarial perturbations in the input lead to small changes in the output as opposed to existing FSS models where the output is unpredictable. In this paper, we make the following contributions:

- We extend SAT for FSS task to handle attacks on both support and query.
- We propose a novel adversarially robust FSS framework, PNODE, that can handle different kinds of adversarial attacks like FGSM [2], PGD [13] and SMIA [33] differing in intensity and design, even without an expensive adversarial training procedure.
- We show the effectiveness of our proposed approach with publicly available multi-organ segmentation datasets like BCV [3], CT-ORG [25] and DE-CATHLON [23] for both in-domain and cross-domain settings on novel classes.

2 Related Works

Neural ODEs: Deep learning models such as ResNets [4] learn a sequence of transformation by mapping input \mathbf{x} to output \mathbf{y} by composing a sequence of transformations to a hidden state. In a ResNet block, computation of a hidden layer representation can be expressed using the following transformation: $\mathbf{h}(t+1) = \mathbf{h}(t) + f_{\theta}(\mathbf{h}(t), t)$ where $t \in \{0, \dots, T\}$ and $\mathbf{h} : [0, \infty] \rightarrow \mathbb{R}^n$. As the

number of layers are increased and smaller steps are taken, in the limit, the continuous dynamics of the hidden layers are parameterized using an ordinary differential equation (ODE) [14] specified by a neural network $\frac{d\mathbf{h}(t)}{dt} = f_{\theta}(\mathbf{h}(t), t)$ where $f : \mathbb{R}^n \times [0, \infty] \rightarrow \mathbb{R}^n$ denotes the non-linear trainable layers parameterized by weights θ and \mathbf{h} represents the n -dimensional state of the Neural-ODE. These layers define the relation between the input $\mathbf{h}(0)$ and output $\mathbf{h}(T)$, at time $T > 0$, by providing solution to the ODE initial value problem at terminal time T . Neural-ODEs are the continuous equivalent of ResNets where the hidden layers can be regarded as discrete-time difference equations.

Recent studies [27,28,31] have applied Neural-ODEs to defend against adversarial attacks. [27] proposes time-invariant steady Neural-ODE that is more stable than conventional convolutional neural networks (CNNs) in the classification setting.

Few-shot Learning: FSL methods seek good generalization and learn transferable knowledge across different tasks with limited data [1,20,21]. Few-shot segmentation (FSS) [24,19,26] aims to perform pixel-level classification for novel classes in a query image when trained on only a few labelled support images. The commonly adopted approach for FSS is based on prototypical networks [6,19,32] that employ prototypes to represent typical information for foreground objects present in the support images. In addition to prototype-based setting, [24] incorporates ‘squeeze & excite’ blocks that avoids the need of pre-trained models for medical image segmentation. [26] uses a relation network [12] and introduced FSS-1000 dataset that is significantly smaller as compared to contemporary large-scale datasets for FSS.

Adversarial robustness: Adversarial attacks for natural image classification has been extensively explored. FGSM [2] and PGD [13] generate adversarial examples based on the CNN gradients. Besides image classification, several attack methods have also been proposed for semantic segmentation [9,10,33,22]. [10] introduced Dense Adversary Generation (DAG) that optimizes a loss function over a set of pixels for generating adversarial perturbations. [15] studied the effects of adversarial attacks on brain segmentation and skin lesion classification. Recently, [33] proposes an adversarial attack (SMIA) for images in medical domain that employs a loss stabilization term to exhaustively search the perturbation space. While adversarial attacks expose the vulnerability of deep neural networks, adversarial training [13,2,8] is effective in enhancing the target model by training it with adversarial samples. However, none of existing methods have explored SAT procedure for few-shot semantic segmentation.

3 Proposed Method

The objective is to build a FSS model robust to various gradient-based attacks on support and query images. Our methodology focuses on two aspects. First, we extend SAT as a defense mechanism. Second, we propose our framework, PNODE, which alleviates existing limitations faced by SAT.

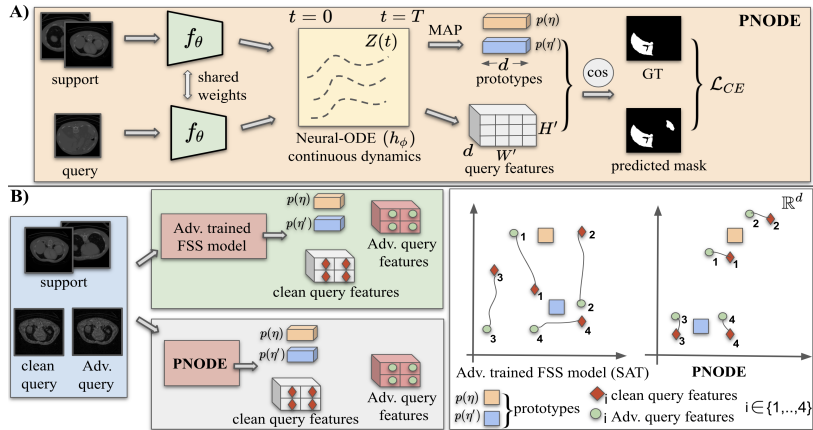


Fig. 1. A) Robust features for query and support images are obtained by the feature extractor followed by the continuous dynamics and integral solutions of a Neural-ODE. Class-wise prototypes are obtained by applying Masked Average Pool (MAP) on support features. Pixel-level cosine similarities of query features with the prototypes provide query mask predictions. **B)** d -dimensional representation of clean and adversarial query features. Adversarial query features lie closer to the clean ones unlike Adversarially trained FSS model (or SAT). In SAT, perturbations from one class may be closer to prototypes of another class (model is confused), while for PNODE, they tend to remain closer.

3.1 Problem setting

FSS setting includes train $\mathcal{D}_{\text{train}}$ and test $\mathcal{D}_{\text{test}}$ datasets having non-overlapping class sets. Each dataset consists of a set of episodes with each episode containing a N -way K -shot task $\mathcal{T}_i = (\mathcal{S}_i, \mathcal{Q}_i)$ where \mathcal{S}_i and \mathcal{Q}_i are support and query sets for the i^{th} episode having class set C_i . Formally, $\mathcal{D}_{\text{train}} = \{(\mathcal{S}_i, \mathcal{Q}_i)\}_{i=1}^{E_{\text{train}}}$ and $\mathcal{D}_{\text{test}} = \{(\mathcal{S}_i, \mathcal{Q}_i)\}_{i=1}^{E_{\text{test}}}$ where E_{train} and E_{test} denote the number of episodes during training and testing. The support set \mathcal{S}_i has K image (\mathcal{I}_S), mask (L_S) pairs per class with a total of N semantic classes i.e. $\mathcal{S}_i = \{(\mathcal{I}_S^k, L_S^k(\eta))\}$ where $L_S^k(\eta)$ is the ground-truth mask for k -th shot corresponding to class $\eta \in C_i$, $|C_i| = N$ and $k = 1, 2, \dots, K$. The query set \mathcal{Q}_i has N_Q image (\mathcal{I}_Q), mask (L_Q) pairs. The FSS model $\mathcal{F}(\cdot)$ is trained on $\mathcal{D}_{\text{train}}$ across the episodes with support sets and query images as inputs, and predicts the segmentation mask $M_Q = \mathcal{F}(\mathcal{S}_i, \mathcal{I}_Q)$ in the i -th episode for query image \mathcal{I}_Q . During testing, the trained model $\mathcal{F}(\cdot)$ is used to predict masks for unseen novel classes with the corresponding support set samples and query images as inputs from $\mathcal{D}_{\text{test}}$.

Further, the trained FSS model is adversarially attacked to record the drop in performance. An adversarial version of a clean sample can be generated by exploiting gradient information from the model $\mathcal{F}(\cdot)$ employing [2]. Specific to the case of FSS, the prediction of query mask not only depends on the query image but also on the information from support set. This enables the attacks to be designed in such a way that either attacked query or support can deteriorate

the query prediction. These perturbations are specifically chosen so that the loss between ground-truth and the predicted masks of the query increases.

3.2 Adversarial Training

To ensure that the segmentation model $\mathcal{F}(\cdot)$ is robust to adversarial perturbations for both support and query images, we extend $\mathcal{D}_{\text{train}}$ in each batch during training with two additional batches generated for the i^{th} episode using update rule from [2] as follows: (a) generate adversarial example for support image \mathcal{I}_S :

$$\mathcal{I}_S^{\text{adv}} = \mathcal{I}_S + \epsilon \cdot \text{sign}(\nabla_{\mathcal{I}_S} \mathcal{L}(\mathcal{F}(\mathcal{S}_i, \mathcal{I}_Q), L_Q(\eta))) \quad (1)$$

(b) generate adversarial example for query image \mathcal{I}_Q :

$$\mathcal{I}_Q^{\text{adv}} = \mathcal{I}_Q + \epsilon \cdot \text{sign}(\nabla_{\mathcal{I}_Q} \mathcal{L}(\mathcal{F}(\mathcal{S}_i, \mathcal{I}_Q), L_Q(\eta))) \quad (2)$$

This is a single-step attack, which minimises the l_∞ norm of the perturbation bounded by parameter ϵ . The detailed procedure of SAT is listed in Algorithm 1.

Algorithm 1 Standard Adversarial Training (SAT) for FSS

Require: Clean training data $\mathcal{D}_{\text{train}} = \{(\mathcal{S}_i, \mathcal{Q}_i)\}_{i=1}^{E_{\text{train}}}$, segmentation network $\mathcal{F}(\cdot)$.

- 1: **for** $i \in \{1, \dots, E_{\text{train}}\}$ **do**
 - 2: Sample episode $\mathcal{E}^{\text{orig}} = \{(\mathcal{S}_i, \mathcal{Q}_i)\}$ from $\mathcal{D}_{\text{train}}$.
 - 3: Calculate gradients w.r.t support and query images using $\mathcal{F}(\cdot)$.
 - 4: Get $\mathcal{E}^S = \{(\mathcal{S}_i^{\text{adv}}, \mathcal{Q}_i)\}$ by perturbing support images using equation 1.
 - 5: Get $\mathcal{E}^Q = \{(\mathcal{S}_i, \mathcal{Q}_i^{\text{adv}})\}$ by perturbing query images using equation 2.
 - 6: **for** $\mathcal{E} \in \{\mathcal{E}^{\text{orig}}, \mathcal{E}^S, \mathcal{E}^Q\}$ **do**
 - 7: Train \mathcal{F} on episode \mathcal{E} .
 - 8: **end for**
 - 9: **end for**
-

SAT requires prior knowledge on the type of adversarial attacks to include the corresponding samples during training which is practically infeasible, compute intensive and also doesn't guarantee robustness to unseen attacks. Our PNODE framework addresses these shortcomings.

3.3 Prototypical Neural ODE (PNODE)

The proposed framework is based on existing prototypical few-shot segmentation models [11,19]. Given an episode i with task $\mathcal{T}_i = (\mathcal{S}_i, \mathcal{Q}_i)$, the feature extractor f_θ generates intermediate feature representations Z_S^k and Z_Q for the support and query images $\mathcal{I}_S^k, \mathcal{I}_Q$. The outputs from the feature extractor f_θ are considered as initial states for the Neural-ODE block at time $t=0$, denoted as $Z_S^k(0), Z_Q(0)$.

The Neural-ODE block consists of hidden layers h_ϕ parameterized by ϕ and its dynamics are governed by h_ϕ which control how the intermediate state

changes at any given time t . The output representation at fixed terminal time $T(T > 0)$ for query features Z_Q is given by $Z_Q(T) = Z_Q(0) + \int_0^T h_\phi(Z_Q(t), t)dt$. Similarly, the output representation at fixed terminal time $T(T > 0)$ for support features Z_S^k are generated. The support feature maps $Z_S^k(T)$ from the Neural-ODE block of spatial dimensions $(H' \times W')$ are upsampled to the same spatial dimensions of their corresponding masks L_S of dimension $(H \times W)$. Inspired by late fusion [19] where the ground-truth labels are masked over feature maps, we employ Masked Average Pooling (MAP) between $Z_S^k(T)$ and $L_S^k(\eta)$ to form a d -dimensional prototype $p(\eta)$ for each foreground class $\eta \in C_i$ as shown:

$$p(\eta) = \frac{1}{K} \sum_k \frac{\sum_{x,y} \{Z_S^k(T)\}^{(x,y)} \cdot \mathbb{1}[\{L_S^k(\eta)\}^{(x,y)} = \eta]}{\sum_{x,y} \mathbb{1}[\{L_S^k(\eta)\}^{(x,y)} = \eta]} \quad (3)$$

where (x, y) are the spatial locations in the feature map and $\mathbb{1}(\cdot)$ is an indicator function. The background is also treated as a separate class and the prototype for it is calculated by computing the feature mean of all the spatial locations excluding the ones that belong to the foreground classes.

The probability map over semantic classes η is computed by measuring the cosine similarity (cos) between each of the spatial locations in $Z_Q(T)$ with each prototype $p(\eta)$ as given by:

$$M_Q^{(x,y)}(\eta) = \frac{\exp(\cos(\{Z_Q(T)\}^{(x,y)}, p(\eta)))}{\sum_{\eta' \in C_i} \exp(\cos(\{Z_Q(T)\}^{(x,y)}, p(\eta')))} \quad (4)$$

The predicted mask M_Q is generated by taking the argmax of $M_Q(\eta)$ across semantic classes. We use Binary Cross Entropy loss \mathcal{L}_{CE} between M_Q and the ground-truth mask for training. For detailed overview of PNODE, refer to Fig.1. During evaluation, PNODE’s robustness against adversarial attacks is attributed to the fact that the integral curves corresponding to the features are non-intersecting. Thus, if a clean sample (support or query) is adversarially perturbed, the integral curves associated with other similar samples constrain the adversarial features to remain bounded in the representation space. Consequently, the perturbed sample’s feature representations are closer to the clean or original feature representations as shown in Fig.1 which leads to accurate predictions of the query masks.

4 Implementation Details

PNODE framework consists of a CNN-based feature extractor followed by a Neural-ODE block consisting of 3 convolutional layers. The architecture of PNODE consists of a total of 14.7M trainable parameters, while PANet and FSS1000 have 14.7M and 18.6M parameters, respectively. The solution for Neural-ODE is obtained by using Runge-Kutta ODE solver [14]. To understand the effect of adversarial training on prototype-based networks, we employ SAT with PANet [19] and name it AT-PANET. It is trained with FGSM with $\epsilon = 0.025$. To test

the trained models, we perturb the support and query images by setting $\epsilon = 0.02, 0.01$ and 0.04 for FGSM, PGD and SMIA, respectively. For the iterative adversarial attacks SMIA and PGD, we take 10 iterations each. These hyperparameters for the attacks were chosen so as to keep the perturbed images human perceptible. We use one A100 GPU to conduct our experiments. For statistical significance, we run each experiment twice and report the mean and standard deviation. All our implementations can be found [here](#).⁴

5 Experiments and Results

We experiment on three publicly available multi-organ segmentation datasets, BCV [3], CT-ORG [25], and Decathlon [23] to evaluate the generalisability of our method. We train on the smaller BCV dataset and use CT-ORG and Decathlon for cross-domain FSS. To have a more uniform size of the test set, we sample 500 random slices per organ from the much larger CT-ORG and Decathlon datasets. For the 3D volumes in all three datasets, we extract slices with valid masks and divide them into fixed train, test, and validation splits. We do not crop the slices class-wise and handle multiple organs in the same slice since cropping in the test set would require labels, leading to an unfair test set evaluation. For baseline models we use PANet [19], FSS1000 [26], SENet [24] and AT-PANET. Of the organs available in these datasets, we report results on Liver and Spleen (as novel classes) due to their medical significance and availability in multiple datasets.

Table 1. 1-shot query attack results for BCV \rightarrow BCV in-domain Liver and Spleen organs (novel classes). The dice scores are rounded off to two decimals.

Method	BCV \rightarrow BCV (Liver)				BCV \rightarrow BCV (Spleen)			
	Clean	FGSM	PGD	SMIA	Clean	FGSM	PGD	SMIA
PANet[19]	.61 \pm .01	.29 \pm .01	.21 \pm .01	.20 \pm .01	.38 \pm .03	.16 \pm .01	.11 \pm .01	.07 \pm .01
FSS1000[26]	.37 \pm .04	.10 \pm .03	.04 \pm .02	.18 \pm .01	.41 \pm .02	.19 \pm .01	.08 \pm .01	.17 \pm .01
SENet[24]	.61 \pm .01	.30 \pm .06	.22 \pm .02	.12 \pm .02	.57 \pm .01	.04 \pm .01	.21 \pm .04	.01 \pm .01
AT-PANet	.65 \pm .01	.35 \pm .03	.27 \pm .02	.36 \pm .01	.46 \pm .01	.32 \pm .08	.19 \pm .03	.11 \pm .01
PNODE	.83\pm.01	.52\pm.02	.46\pm.01	.38\pm.03	.60\pm.01	.36\pm.01	.27\pm.03	.20\pm.02

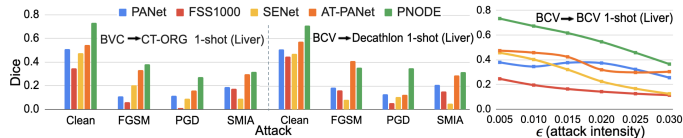
As shown in Table 3, PNODE outperforms all of our baselines by atleast 27%, 48%, 70% and 5% on clean, FGSM, PGD and SMIA attacks respectively for BCV in-domain Liver setting. While PNODE provides a better defense against the adversarial attacks, it also outperforms the baselines for clean samples. This indicates that PNODE also learns a better representation space of unperturbed support and query samples which is attributed to the continuous dynamics of the Neural-ODE. With small perturbations, the integral curves with respect to

⁴ https://github.com/prinshul/Prototype_NeuralODE_Adv_Attack

Table 2. 3-shot query attack results for Liver BCV in-domain and BCV \rightarrow CT-ORG cross-domain settings. The dice scores are rounded off to two decimals.

Method	BCV \rightarrow BCV (Liver)				BCV \rightarrow CT-ORG (Liver)			
	Clean	FGSM	PGD	SMIA	Clean	FGSM	PGD	SMIA
PANet[19]	.67 \pm .01	.38 \pm .01	.31 \pm .01	.16 \pm .01	.60 \pm .01	.23 \pm .01	.21 \pm .01	.17 \pm .01
FSS1000[26]	.49 \pm .04	.15 \pm .01	.05 \pm .01	.19 \pm .03	.14 \pm .02	.03 \pm .01	.01 \pm .01	.08 \pm .01
AT-PANet	.69 \pm .01	.36 \pm .09	.39 \pm .01	.23 \pm .01	.64 \pm .03	.09 \pm .05	.21 \pm .02	.18 \pm .01
PNODE	.76\pm.02	.53\pm.01	.52\pm.01	.39\pm.02	.68\pm.01	.43\pm.02	.42\pm.01	.31\pm.02

the perturbed samples are sandwiched between the curves that correspond to the neighbouring samples ensuring that outputs of the perturbed samples do not change drastically. This is not the case with traditional CNNs, as there are no such intrinsic constraints [27]. To further show the Neural-ODE’s role in robustness, we conduct a set of ablation studies. Upon removing the Neural-ODE block from PNODE, maintaining the remaining architecture and training procedure, we observed 0.41, 0.36, 0.36 and 0.31 units of drop in performance for clean, FGSM, PGD and SMIA, respectively. Further, using SAT made this model more robust, but PNODE outperformed it by 0.28, 0.19, 0.20 and 0.31 units, respectively. An interesting observation is that the baseline results tend to perform well for some attacks, while fail for others. For example, SENet [24] does very well on PGD [13] attack with a dice of 0.21, but performs very poorly on SMIA [33]. PNODE, on the other hand performs consistently across the different attacks. As can be seen in Fig.2, PNODE also performs well on a wider range of attack intensities. Some other experimental analyses in the cross-domain setting can be seen in Fig.2, which follow similar patterns with consistently better performance of PNODE. We also perform experiments on the 3-shot setting in Table 4. While there is a consistent drop between in-domain and cross-domain performance of all models, the drops corresponding to PNODE are relatively smaller. Thus, similar to distribution shifts between clean and perturbed samples, PNODE is also robust to cross-domain distribution shifts. We visualise

**Fig. 2.** Performance of models for attacks on BCV \rightarrow CT-ORG (left), BCV \rightarrow Decathlon (middle) and for different intensities of FGSM (right), on Liver 1-shot.

the predictions by each of these models for the different attacks in Fig.3. For the clean samples, PANet, AT-PANet and PNODE are visually very similar, while FSS1000 and SENet have relatively poorer performance. For FGSM, AT-PANet performs much better than PANet, most likely because of encountering similar

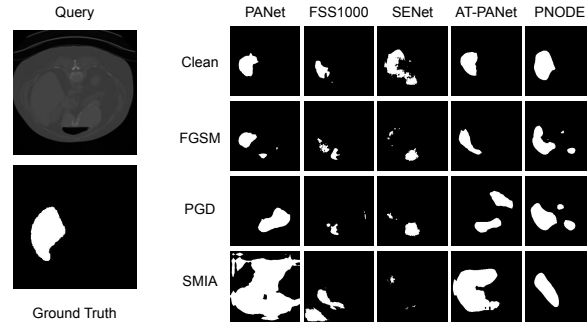


Fig. 3. Predicted masks by different models for different attacks. On the left are the query sample being tested and its ground-truth.

data during training. For PGD, all of PANet, FSS1000, SENet and AT-PANet predict shapes that resemble the true organ, but are at wrong locations. PNODE is able to localise the organ better. For SMIA, all the predictions are poor and PNODE is the only one even closely resembling the actual labels. For additional results, please refer to the supplementary material.

6 Conclusion

Defense against adversarial attacks on few-shot segmentation models is of utmost importance as these models are data-scarce. With their applications in the medical domain, it is critical to provide robust mechanisms against attacks of varying intensity and design. Although adversarial training can alleviate the risk associated with these attacks, the training procedure’s computational overhead and poor generalizability render it less favourable as a robust defense strategy. We overcome its limitations by employing Neural-ODEs to propose adversarially robust prototypical few-shot segmentation framework PNODE that stabilizes the model against adversarial support and query attacks. PNODE is shown to have better generalization abilities against attacks while maintaining performance on clean examples. To the best of our knowledge, we are the first to study effects of different adversarial attacks on few-shot segmentation models and provide a robust defense strategy that we hope will help the medical community.

References

1. Li Fei-Fei, Rob Fergus, Pietro Perona. One-shot learning of object categories, IEEE TPAMI, vol. 28, 2006.
2. Ian J. Goodfellow, Jonathon Shlens, Christian Szegedy. Explaining and harnessing adversarial examples. In ICLR, 2015.
3. Bennett Landman, Zhoubing Xu, Juan Eugenio Iglesias, Martin Styner, Thomas Robin. Langerak, Arno Klein. Miccai multi-atlas labeling beyond the cranial

- vault-workshop and challenge. In MICCAI Multi-Atlas Labeling Beyond Cranial Vault—Workshop Challenge, 2015.
4. Kaiming He, Xiangyu Zhang, Shaoqing Ren, Jian Sun. Deep Residual Learning for Image Recognition. In CVPR, 2016.
 5. Alexey Kurakin, Ian J. Goodfellow, Samy Bengio. Adversarial examples in the physical world. ICLR (Workshop) 2017.
 6. Jake Snell, Kevin Swersky, Richard S. Zemel. Prototypical networks for few-shot learning. In NeurIPS, 2017.
 7. Sachin Ravi, Hugo Larochelle. Optimization as a model for few-shot learning. In ICLR, 2017.
 8. Alexey Kurakin, Ian J. Goodfellow, Samy Bengio. Adversarial machine learning at scale. In ICLR, 2017.
 9. Seyed-Mohsen Moosavi-Dezfooli, Alhussein Fawzi, Omar Fawzi, Pascal Frossard. Universal adversarial perturbations. In CVPR, 2017.
 10. Cihang Xie, Jianyu Wang, Zhishuai Zhang, Yuyin Zhou, Lingxi Xie, Alan Yuille. Adversarial examples for semantic segmentation and object detection. In ICCV, 2017.
 11. Nanqing Dong, Eric P. Xing. Few-shot semantic segmentation with prototype learning. In BMVC, 2018.
 12. Flood Sung, Yongxin Yang, Li Zhang, Tao Xiang, Philip H.S. Torr, Timothy M. Hospedales. Learning to compare: Relation network for few-shot learning. In CVPR, 2018.
 13. Aleksander Madry, Aleksandar Makelov, Ludwig Schmidt, Dimitris Tsipras, Adrian Vladu. Towards deep learning models resistant to adversarial attacks. In ICLR, 2018.
 14. Ricky T. Q. Chen, Yulia Rubanova, Jesse Bettencourt, David Duvenaud. Neural ordinary differential equations. In NeurIPS, 2018.
 15. Magdalini Paschali, Sailesh Conjeti, Fernando Navarro, Nassir Navab. Generalizability vs. Robustness: Investigating medical imaging networks using adversarial examples. In MICCAI, 2018.
 16. Anurag Arnab, Ondrej Miksik, Philip H.S. Torr. On the robustness of semantic segmentation models to adversarial attacks. In CVPR, 2018.
 17. Hongyang Zhang, Yaodong Yu, Jiantao Jiao, Eric Xing, Laurent El Ghaoui, Michael Jordan. Theoretically principled trade-off between robustness and accuracy. In ICML, 2019.
 18. Huan Zhang, Hongge Chen, Zhao Song, Duane Boning, Inderjit Dhillon, Cho-Jui Hsieh. The limitations of adversarial training and the blind-spot attack. In ICLR, 2019.
 19. Kaixin Wang, Jun Hao Liew, Yingtian Zou, Daquan Zhou, Jiashi Feng. Panet: Few-shot image semantic segmentation with prototype alignment. In ICCV, 2019.
 20. Amy Zhao, Guha Balakrishnan, Frédo Durand, John V. Guttag, Adrian V. Dalca. Data augmentation using learned transformations for one-shot medical image segmentation. In CVPR, 2019.
 21. Cheng Ouyang, Konstantinos Kamnitsas, Carlo Biffi, Jinming Duan, Daniel Rueckert. Data efficient unsupervised domain adaptation for cross-modality image segmentation. In MICCAI, 2019.
 22. Utku Ozbulak, Arnout Van Messem, Wesley De Neve. Impact of adversarial examples on deep learning models for biomedical image segmentation. In MICCAI, 2019.
 23. Amber L. Simpson, et al. 2019. A large annotated medical image dataset for the development and evaluation of segmentation algorithms. arXiv preprint arXiv:1902.09063.

24. Abhijit Guha Roy, Shayan Siddiqui, Sebastian Pölsterl, Nassir Navab, Christian Wachinger. ‘Squeeze & Excite’ Guided few-shot segmentation of volumetric images. In *MedIA*, vol. 59, 2020.
25. Blaine Rister, Darvin Yi, Kaushik Shivakumar, Tomomi Nobashi, Daniel L. Rubin. CT-ORG, a new dataset for multiple organ segmentation in computed tomography. In *Scientific Data*, 2020. <https://doi.org/10.1038/s41597-020-00715-8>.
26. Xiang Li, Tianhan Wei, Yau Pun Chen, Yu-Wing Tai, Chi-Keung Tang. FSS-1000: A 1000-class dataset for few-shot segmentation. In *CVPR*, 2020.
27. Hanshu Yan, Jiawei Du, Vincent Y. F. Tan, Jiashi Feng. On robustness of neural ordinary differential equations. In *ICLR*, 2020.
28. Xuanqing Liu, Tesi Xiao, Si Si, Qin Cao, Sanjiv Kumar, Cho-Jui Hsieh. How does noise help robustness? Explanation and exploration under the neural sde framework. In *CVPR*, 2020.
29. Micah Goldblum, Liam Fowl, Tom Goldstein. Adversarially robust few-shot learning: A meta-learning approach. In *NeurIPS*, 2020.
30. Sanglee Park, Jungmin So. On the effectiveness of adversarial training in defending against adversarial example attacks for image classification. In *Applied Sciences*, 10(22):8079, 2020. <https://doi.org/10.3390/app10228079>.
31. Qiyu Kang, Yang Song, Qinxu Ding, Wee Peng Tay. Stable neural ode with Lyapunov-stable equilibrium points for defending against adversarial attacks. In *NeurIPS*, 2021.
32. Hao Tang, Xingwei Liu, Shanlin Sun, Xiangyi Yan, Xiaohui Xie. Recurrent mask refinement for few-shot medical image segmentation. In *ICCV*, 2021.
33. Gege Qi, Lijun Gong, Yibing Song, Kai Ma, Yefeng Zheng. Stabilized medical image attacks. In *ICLR*, 2021.
34. Xiaogang Xu, Hengshuang Zhao, Jiaya Jia. Dynamic divide-and-conquer adversarial training for robust semantic segmentation. In *ICCV*, 2021.

A Additional Results

Table 3. 1-shot *support* attack results for BCV \rightarrow BCV in-domain Liver and Spleen organs (novel classes). The dice scores are rounded off to two decimals.

Method	BCV \rightarrow BCV (Liver)				BCV \rightarrow BCV (Spleen)			
	Clean	FGSM	PGD	SMIA	Clean	FGSM	PGD	SMIA
PANet	.61 \pm .01	.17 \pm .06	.39 \pm .01	.11 \pm .01	.39 \pm .05	.17 \pm .02	.10 \pm .02	.03 \pm .01
AT-PANet	.65 \pm .02	.19 \pm .07	.30 \pm .15	.11 \pm .01	.49 \pm .05	.42 \pm .03	.32 \pm .06	.03 \pm .01
PNODE	.82\pm.03	.63\pm.17	.72\pm.02	.17\pm.05	.60\pm.02	.43\pm.01	.38\pm.02	.05\pm.01

B Additional Plots and Visualisations

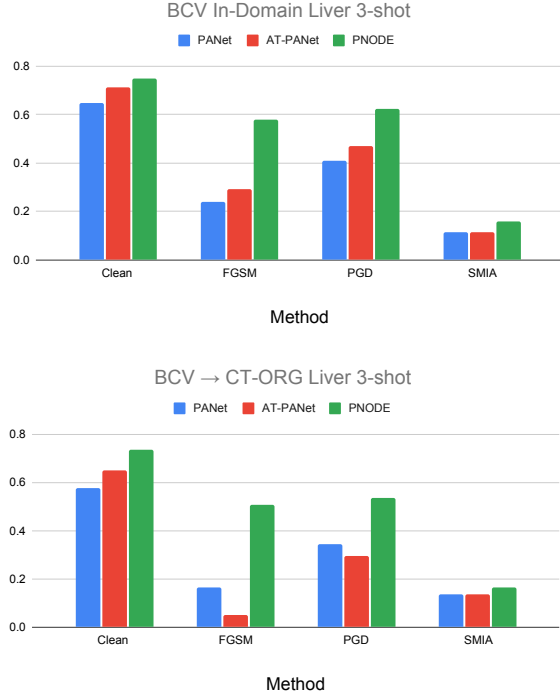


Fig. 4. Performance of models for *support* attacks on BCV \rightarrow BCV in-domain and BCV \rightarrow CT-ORG cross-domain Liver 3-shot.

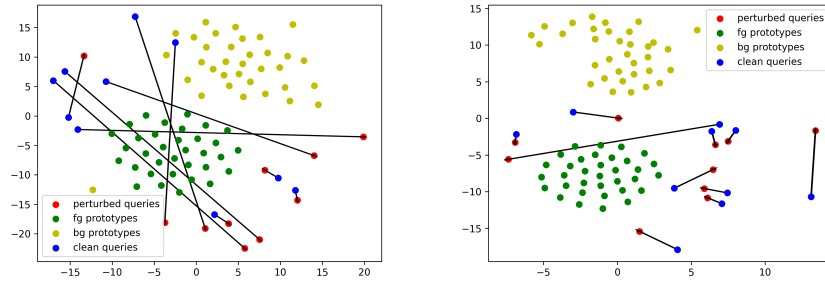


Fig. 5. t-SNE visualisations of clean and perturbed queries with foreground and background prototypes for PANet (left) and PNODE (right) (BCV Liver 1-shot).

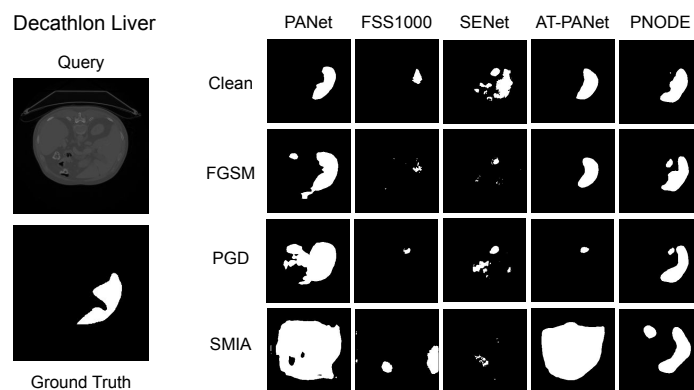


Fig. 6. Predicted masks by different models for different attacks on Decathlon Liver 1-shot. On the left are the query sample being tested and its ground-truth.

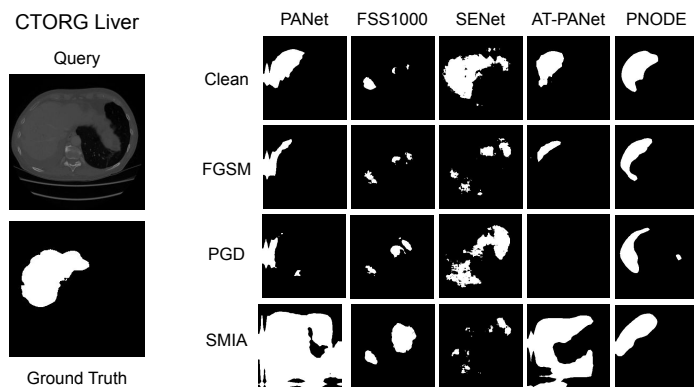


Fig. 7. Predicted masks by different models for different attacks on CT-ORG Liver 1-shot. On the left are the query sample being tested and its ground-truth.

Table 4. 1-shot *support* attack results for Liver BCV \rightarrow Decathlon and BCV \rightarrow CT-ORG cross-domain settings. The dice scores are rounded off to two decimals.

Method	BCV \rightarrow Decathlon (Liver)				BCV \rightarrow CT-ORG (Liver)			
	Clean	FGSM	PGD	SMIA	Clean	FGSM	PGD	SMIA
PANet	.53 \pm .01	.15 \pm .01	.35 \pm .02	.13 \pm .01	.52 \pm .01	.20 \pm .05	.43 \pm .02	.14 \pm .01
AT-PANet	.57 \pm .01	.14 \pm .04	.31 \pm .06	.13 \pm .01	.56 \pm .01	.12 \pm .02	.32 \pm .08	.14 \pm .01
PNODE	.65\pm.01	.49\pm.01	.55\pm.01	.16\pm.02	.66\pm.01	.51\pm.03	.50\pm.04	.22\pm.04